Research article

A simple method to set the spray properties for flame spray pyrolysis production of nanoparticles

Mustafi A. Alhaleeb, Nesrin E. Machin [*]

Department of Chemical Engineering and Applied Chemistry, Atılım University, Ankara, Turkey

A B S T R A C T

The most critical part of the flame spray pyrolysis (FSP) process is the nozzle, since it plays a key role in setting the spray properties. In this study, we developed an approach to adjust the nozzle throat gap size for a desired dispersion gas flow rate and upstream pressure, based on the external size and shape of a two phase external mixing nozzle. An equation was derived and validated by comparing the predicted gas flow rates with the data provided in a commercial nozzle supplier chart. Experiments were also conducted in our lab-scale FSP reactor to test the validity of the predictions. The approach developed here was found to closely predict the gap size necessary to pass the required dispersion gas flow at a desired pressure drop. Error in predictions was found to be less than 3% at an upstream pressure range of 3–10 bars. The isentropic flow assumption for perfect gases across the convergent-divergent nozzle was found to fail below 2 bars, consistent with the theory applied. By using the method here, the nozzle setting for a desired operation in an FSP process can be easily done, minimizing the time-consuming trial and error steps needed otherwise.

1. Introduction

Flame Spray Pyrolysis (FSP) is a versatile and cost-efficient production process for nanoparticles, which relies on the oxidation of liquid raw materials containing metal or transition metal compounds at flame temperatures. Product nanoparticles are formed within milliseconds, and collected as a dry powder on a filter. An FSP reactor consists of 3 main parts; a two-fluid nozzle for liquid precursor delivery and atomization, which is located in the center of a burner, a premixed or diffusion burner as an ignition source for the liquid precursor, and a downstream filtering system for nanoparticle product collection. Configuration of an FSP system affects the performance of the process and product powder characteristics. Liquid droplets' diameter in the spray as well as droplets and particles residence times in the flame effects the chemical and morphological structures of the nanomaterial produced. This process can be used to produce different types of nanoparticles of almost all the elements in the periodic table [1].

Flow regime at the nozzle throat depends on the nozzle type and configuration, ultimately changing the spray properties. FSP typically employs two-phase fluid nozzles, where the liquid is atomised to droplets by a high-velocity dispersion gas. These nozzles can be further categorized into external and internal mixing types, depending on the mixing

location of the two phases. The former types are preferred in FSP processes [2, 3, 4, 5, 6, 7, 8, 9, 10, 11]. A typical external mixing two phase nozzle configuration consists of two separate bodies: a fixed inner body (including the liquid delivery tube) and a movable body (dispersion gas cap, or air cap) [12]. By turning the air cap clockwise or counter-clockwise, the gap size decreases or increases, respectively.

A representative sketch of the nozzle top drawn with the Ansys Fluent (v.19) Space Claim drawing package is shown in Figure 1. The nozzle throat is formed by connecting the fixed inner body with the movable top part, which sets the size of the gas exit gap (X), depending on the height of the distance shown in the figure as DR. A convergent-divergent configuration of the nozzle forms when the dispersion gas cap is connected. Gap size at the throat can be adjusted by moving the gas cap up or down.

In this study, a mathematical relationship between the measurable external geometry and the internal throat gap size (X) of a commercial nozzle was developed [12]. Lowest and highest standard settings (gap sizes) correspond to position 1 (P1) and position max (Pmax), respectively. Gap size X cannot be measured after inner and top parts of the nozzle are connected, and it is needed to calculate the cross-sectional area (A) to set the nozzle position for a desired gas flow rate at a required pressure drop. This approach is used for the production of
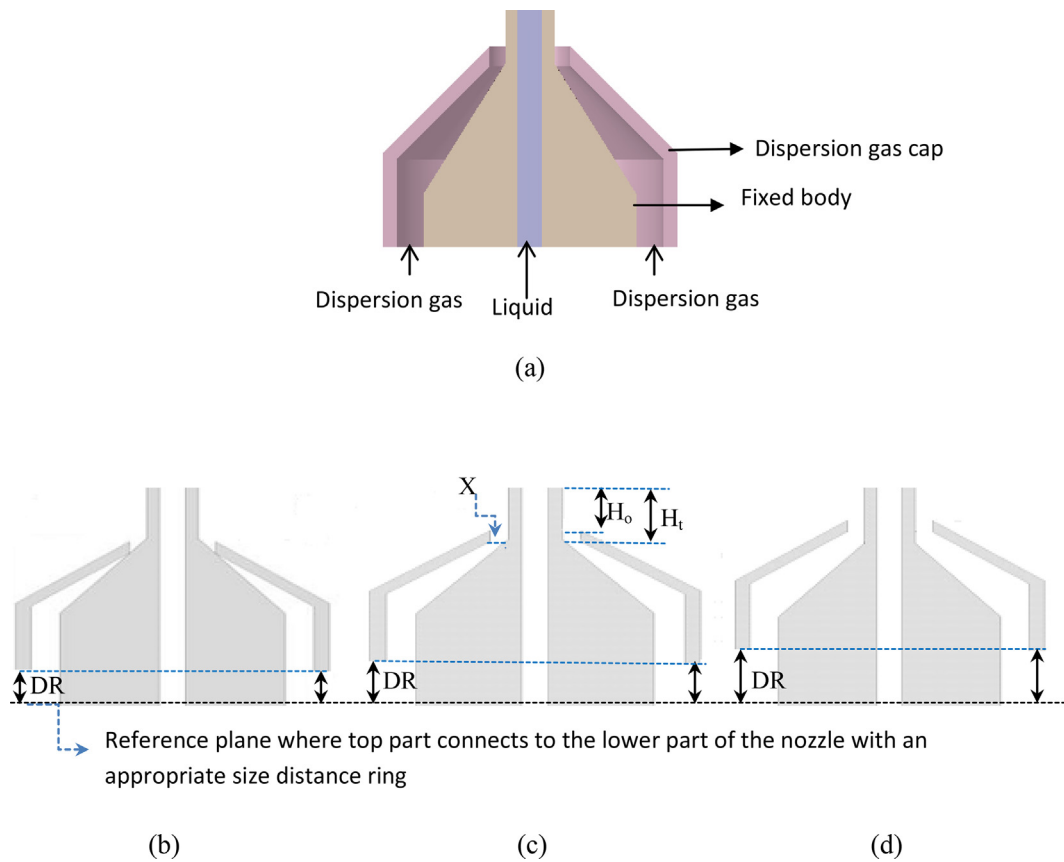
Figure 1. 3D view (a), and cross sectional view of the nozzle tip at closed (b), intermediate (c), and higher (d) positions (DR, distance ring height, H_t; liquid delivery tube extension length, H_o; liquid delivery tube height above air cap).

nano-TiO$_2$ in an FSP system in our laboratory. Details of the FSP set-up can be found in references [13, 14]. The nozzle used in this work came with a standard distance ring (DR) on the air cap, which guaranteed after disassembly and assembly the correct air-cap position number 4 (P4) with a distance ring height of 3.01mm [15]. In order to produce TiO$_2$ at 5 to 10 LPM oxygen dispersion gas flow rates with 1–1.5 bar pressure drops for Schlick 970, a nozzle position of less than P1 was required, as can be seen in Figure 2 [15]. Clearly we needed to work at positions that were

less than the manufacturer's standard production could provide, but there was no guidance in the manual, other than the instruction to use the trial and error method to find the required position. Therefore, we had manufactured distance rings, ranging from 2.20 to 2.99 mm, with 0.01 mm increment(s) to adjust the pressure drop for required dispersion gas flow rates that would provide linear gas velocities at or above sonic speed to obtain a fine spray.

Fabricating new distance rings was costly, and time consuming due to the number of distance rings required for the trial and error method to adjust the pressure drop for a desired gas flow rate. While going through the trial and error steps for the correct distance ring size, we developed an approach to predict the distance ring height for a required pressure drop to save time and cost for the future experimental studies. As depicted in Figure 1, when the dispersion gas cap (or air cap) is turned clockwise (forwards), X will be reduced, H_o will increase while DR decreases. Thus, a relationship between X, H_o and DR can be derived by using the geometrical relationships between the measurable outer dimensions. This relationship can be used as a tool for external-mixing gas-assisted atomisers to calculate the gap size at any dispersion gas flow rate and applied pressure, based on the nozzle outer dimensions, therefore eliminating the time consuming trial and error procedures during the experiments. Additionally, commercial nozzle producers do not provide the information concerning the inner nozzle dimensions, due to the "know how" rights. However, nozzle gap size is not only important for experimental studies, it is also an important parameter in drawing and meshing the geometry in computational fluid dynamics modelling of FSP processes. Therefore, this approach provides the necessary information in setting up the computational domain as well. Moreover, by using the equation derived, an existing commercial nozzle can be utilized beyond the data range provided in standard nozzle charts. Validation of the equations was performed by comparing the flow rates predicted in this study with the supplier charts for applied pressures up to 10 bars.
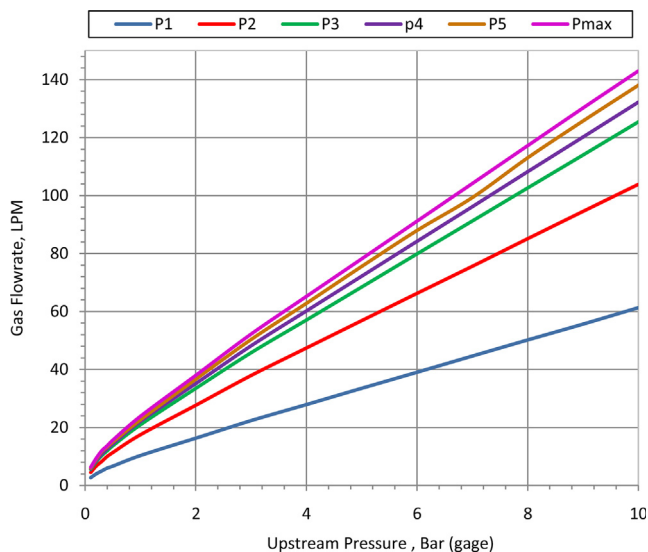

Figure 2. Gas flow rates versus pressure drop readings at throat gaps P1 to Pmax.

2. Theoretical background

2.1. Calculation of the minimum cross section area

In an external mixing two phase nozzle, dispersion gas first passes vertically through the constant cross-section annulus, and subsequently the reducer, where the cross-section gradually decreases to its minimum at the nozzle throat (convergent part). Gas finally passes through the expanded cross-sectional area (divergent part). In convergent configuration, the maximum gas velocity in the throat cannot be higher than 330 m/s (sonic regime) for air at an applied pressure. After the sonic condition is reached, the duct then becomes choked and cannot carry any additional mass flow, unless the throat gap size is widened [16]. As the applied pressure is increased above a critical value, flow transitions to supersonic in the divergent section. Ma number is a measure of defining the flow regime, and effects the relative velocity between the liquid and dispersion gas, which is a key factor governing the size of the droplets. It is the ratio of the dispersion gas linear velocity to the speed of sound of the same gas at room temperature and sea level. In an FSP process, flow rate of the dispersion gas therefore is an important operational parameter that ensures the appropriate dispersion gas velocity required for the atomisation process. For external mixing two-phase nozzles, initial droplet size (ID) is calculated by using the correlation by Lefebvre et al. [17] as,

$$ID = 51 \, d_n \, Re^{-0.39} We^{-0.18} \left(\frac{m_{mix}}{m_{gas}} \right)^{0.29} \tag{1}$$

The droplet Reynolds (Re) and Weber (We) numbers are defined as,

$$Re = \frac{\rho_{mix} \, d_n \left(v_{gas} - v_{mix} \right)}{\mu_{mix}} \text{ and We} = \frac{\rho_{mix} d_n \left(v_{gas} - v_{mix} \right)^2}{\gamma_{mix}}$$

Eq. (1) reveals the dependency of the liquid droplet size to various parameters as,

$$ID \propto \mu_{mix}^{0.39}, \, \gamma_{mix}^{0.18}, \, m_{mix}^{0.29}, \, \frac{1}{\rho_{mix}^{57}}, \, \frac{1}{\left(v_{gas} - v_{mix} \right)^{0.75}}, \text{ and } \frac{1}{\left(m_{gas} \right)^{0.29}}$$

It can be deduced that the relative velocity between the liquid and atomisation gas is a key factor that governs the atomisation quality, such that the relative velocity between the gas and the liquid should be increased to decrease the initial droplet size. Initial droplet size can be reduced by 40% by increasing the pressure drop, and doubling the relative velocity at a constant gas flow rate. On the other hand, it can only be reduced by 15% if the dispersion gas flow rate is doubled under a constant pressure drop. To attain a good atomisation quality (fine spray), the nozzle air cap setting must be adjusted to increase the relative velocity as high as possible for a given pressure drop.

Physical properties of the gas at the throat that are required to find the cross section area can be calculated by combining the isentropic approximation with the assumption of adiabatic flow for a perfect gas [16].

$$\frac{T_0}{T} = 1 + \frac{\gamma - 1}{2} Ma^2 \tag{2}$$

Pressure and density ratios can be computed from power-law relations for an isentropic perfect gas.

$$\frac{P_0}{P} = \left(\frac{T_0}{T} \right)^{\frac{\gamma}{\gamma-1}} \tag{3}$$

$$\frac{\rho_0}{\rho} = \left(\frac{T_0}{T} \right)^{\frac{1}{\gamma-1}} \tag{4}$$

$$\frac{a_0}{a} = \left(\frac{T_0}{T} \right)^{\frac{1}{2}} \tag{5}$$

Figure 3. Nozzle throat geometry between minimum and maximum air cap positions.

For sonic flow at Ma = 1.0, the critical properties are denoted by asterisks p*, ρ*, a*, T*, and γ = 1.4 for air and oxygen, common dispersion gases used in FSP processes. Eqs. (2), (3), (4), and (5) become:

$$\frac{T^*}{T_0} = \frac{2}{\gamma + 1} = 0.8333 \tag{6}$$

$$\frac{P^*}{P_0} = \left(\frac{2}{\gamma + 1} \right)^{\frac{\gamma}{\gamma-1}} = 0.5283 \tag{7}$$

$$\frac{\rho^*}{\rho_0} = \left(\frac{2}{\gamma + 1} \right)^{\frac{1}{\gamma-1}} = 0.6339 \tag{8}$$

$$\frac{a^*}{a_0} = \left(\frac{2}{\gamma + 1} \right)^{\frac{1}{2}} = 0.9129 \tag{9}$$

When the upstream pressure is raised above the critical pressure (P*/0.5283), discharge velocity of the gas from nozzle increases beyond the speed of sound and becomes supersonic. When the critical conditions are reached, the maximum discharge mass flow rate can be calculated from the continuity equation,

$$\dot{m}_{max} = \rho^* A_{min} V^* \tag{10}$$

where V* is critical velocity (speed of sound),

$$V^* = \left(\frac{2\gamma \, R_g \, T_o}{\gamma + 1} \right)^{\frac{1}{2}} \tag{11}$$

Combining Eqs. (8) and (10) and (11) gives:

$$\dot{m} = P_u \left(\frac{\gamma \, M}{R \, T_u} \right)^{\frac{1}{2}} \left(\frac{2}{\gamma + 1} \right)^{\frac{\gamma+1}{2(\gamma-1)}} A_{min} \tag{12}$$

where the maximum mass flow ṁ is proportional to the critical cross-sectional area A_{min} and the absolute upstream pressure P_u. Dividing Eq. (12) by the standard density of the dispersion gas and rearranging gives,

$$A_{min} = \frac{Qs}{\frac{P_u}{\rho u} \left(\frac{\gamma \, M}{R \, T_u} \right)^{\frac{1}{2}} \left(\frac{2}{\gamma+1} \right)^{\frac{\gamma+1}{2(\gamma-1)}}} \tag{13}$$

Eq. (13) can be used to calculate the value of A_{min} for an upstream pressure above the critical pressure. This equation can also be used to find the required dispersion gas flow rate Q_s for a desired pressure drop across the nozzle throat.

Table 1. External measurable dimensions of the nozzle Schlick 970 Form 4 [12].

Symbol	Description	Dimension, mm
H_t	Liquid delivery tube extension length	2.50
H_{max}	Height at zero gas flow	2.64
r_a	Air cap inner radius	0.95
r_c	Liquid delivery tube outer radius	0.80
t	Air cap wall thickness	0.50
β	Angle of inclination for the air cap	45°
θ	Angle of inclination for the liquid tube	32°

2.2. Derivation of the relationship between the nozzle gap and the air cap position

Nozzle geometry and the notations for external dimensions used in the derivation are shown in Figure 3.

This sketch represents the axisymmetric cross-section of an external mixing nozzle after connecting the liquid delivery tube and air cap parts used in this study [12]. In this figure, H_{max}, H_t, r_c, θ, β, r_a, and t are easily measurable external dimensions, and are given in Table 1.

Liquid flows through the delivery tube in the center, and dispersion gas through a convergent-divergent flow passage formed between the liquid delivery tube and the air cap. When the air cap tip touches the liquid tube body (position I), it is the maximum downward movement of the air cap (clockwise turn), no dispersion gas can pass at this position, and we have referred to this as the "zero flow position". Turning the air cap counter-clockwise will move it up in the Y direction, and increase the gap perpendicular to the gas flow (X_p), which cannot be measured. Any position in between position I and III will have an area that is larger than 0 and less than or equal to A_{III}:

$$A_{III} = \pi\left(r_a^2 - r_c^2\right) \tag{14}$$

After position III, the air cap tip will move up beyond the conical section of the liquid delivery tube, and the area perpendicular to gas flow in this region (e.g. IV and V) will be higher than A_{III}. Position V is shown as the maximum movement of the air cap, and after this position, mixing of the gas and the liquid phases would occur internally (internal-mixing nozzle). A relationship between A_{min} and H_o (liquid tube height above the air cap) is developed by considering the two limiting cases. Case 1 considers the air cap positions that are below the conical section of the liquid delivery tube (III), and Case 2 considers the air cap positions above the conical section. Derivation for both cases will be shown next.

Case–I. Air cap movement on the liquid insert cone:
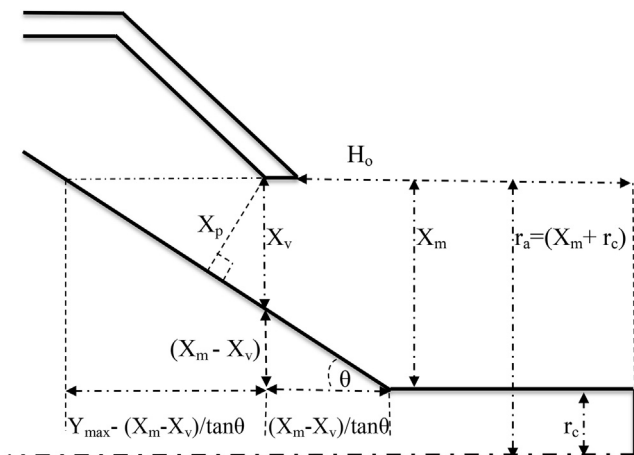
Figure 4. Nozzle configuration for CaseI.

Cross-sectional area perpendicular to the gas flow is:

$$A = \frac{\pi}{4}\left(D_a^2 - \left(D_a - 2X_p\right)^2\right) \tag{15}$$

In this configuration, X_v is the vertical gap between the air cap and the liquid delivery outer tube surface, and $0 \leq X_v \leq X_m$. Eq. (15) can be solved for X_P as,

$$X_p^2 - \pi D_a X_p + A = 0 \tag{16}$$

Solution to Eq. (16) yields;

$$X_p = \frac{D_a}{2} - \frac{\sqrt[2]{D_a^2 - \frac{4}{\pi}A}}{2} \tag{17}$$

The root with the positive sign in Eq. (17) is omitted, because it would yield an X_p higher than the inner radius of the air cap.

Now X_v can be found as,

$$X_v = X_P/\sin(90 - \theta) \tag{18}$$

$$X_v = \left(D_a \Big/ 2 - \sqrt{D_a^2 - 4A/\pi}\Big/ 2\right)\Big/ \sin(90 - \theta) \tag{19}$$

The nozzle geometry and dimensions displayed in Figure 4 then can be used to obtain the liquid tube height above the air cap as:

$$H_o = H_{max} - \left(Y_{max} - \left(X_m - X_v\right)/\tan\theta\right) \tag{20}$$

Eq. (20) relates the un-measurable dimension X_v to a measurable quantity H_o within the limits of Case I as:

$$t \leq H_0 < Y_{max}$$

$$Y_{max} = X_m/\tan\theta$$

$$H_0 = H_{max} - \left\{Y_{max} - \left[X_m - \left(\frac{D_a}{2} - \frac{\sqrt{D_a^2 - 4A/\pi}}{2}\right)\Big/ \sin(90 - \theta)\right]\Big/ \tan\theta\right\} \tag{21}$$

In order to adjust the nozzle throat gap X and maintain the flow at the nozzle throat away from the choking conditions, area in Eq. (21) is replaced with A_{min}:

$$H_0 = H_{max} - \left\{Y_{max} - \left[X_m - \left(\frac{D_a}{2} - \frac{\sqrt{D_a^2 - 4A_{min}/\pi}}{2}\right)\Big/ \sin(90 - \theta)\right]\Big/ \tan\theta\right\} \tag{22}$$

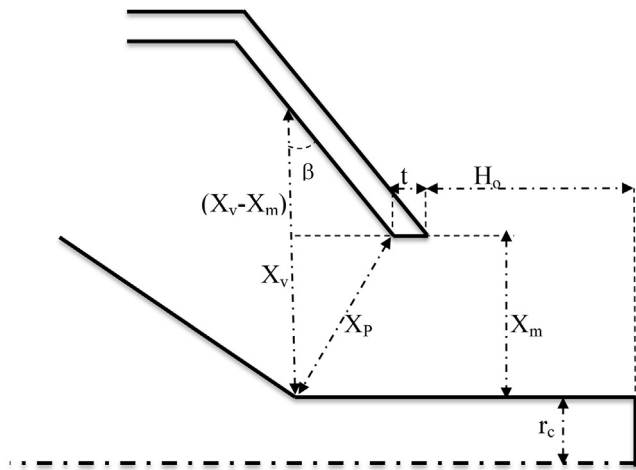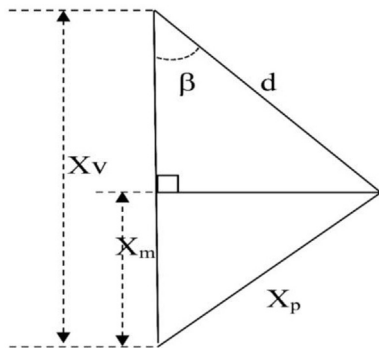**Case–II.** Air cap movement beyond the liquid insert cone:

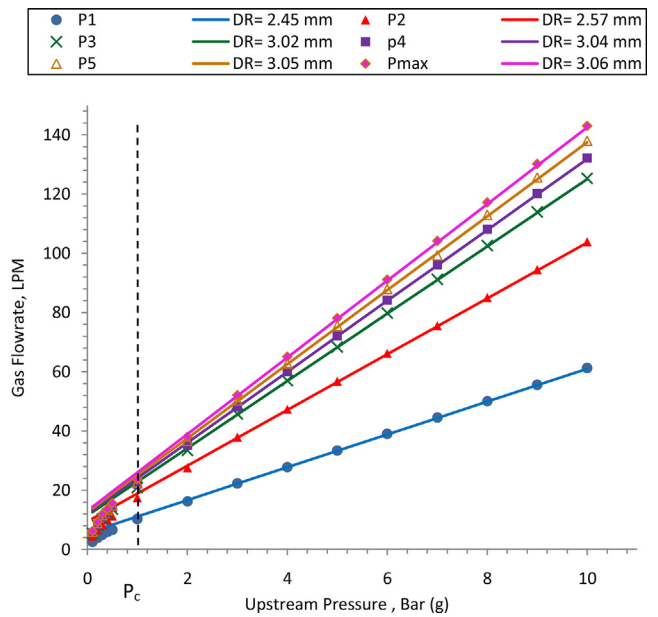**Figure 5.** Nozzle configuration for CaseII.

Figure 7. Dispersion gas flow rates as a function of upstream pressure at positions P1 to Pmax (Lines-predictions, symbols nozzle supplier data [15]).

Here, the cross-sectional area perpendicular to the gas flow is:

$$A = \frac{\pi}{4}\left((2X_P + D_c)^2 - D_c^2\right) \tag{23}$$

Eq. (23) can be arranged to the quadratic formula for X_P as:

$$\pi X_p^2 + \pi D_c X_p - A = 0 \tag{24}$$

The valid root for the equation after omitting the negative sign (because it will produce a negative value for X_p), is found as:

$$X_P = -D_c/2 + \sqrt{D_c^2 + 4A/\pi}/2 \tag{25}$$

In this Case, the relationship between X_V and X_P can be found by applying the "law of cosines" for the triangle in Figure 5.

$$X_p^2 = d^2 + X_p^2 - 2dX_v \cos\beta \tag{26}$$

From Figure 6, it can be seen that, $d = (X_v - X_m)/\cos\beta$.

Figure 6. Triangle geometry.

Substituting d in Eq. (26):

$$X_p^2 = [((X_v - X_m)/\cos\beta)]^2 + X_v^2 - 2X_v\cos\beta[(X_v - X_m)/\cos\beta] \tag{27}$$

Eq. (27) can be arranged to the quadratic equation to find X_v:

$$X_v^2[1/(\cos\beta)^2 - 1] + X_V[2X_m - 2X_m/(\cos\beta)^2] + [X_m^2/(\cos\beta)^2 - X_p^2] = 0 \tag{28}$$

To simplify the equation, the constants are grouped together as,

$$a = [1/(\cos\beta)^2 - 1] \quad b = [2X_m - 2X_m/(\cos\beta)^2] \quad c = [X_m^2/(\cos\beta)^2 - X_p^2]$$

The solution to Eq. (28) after omitting the root with the negative sign (because it would result in X_V less than X_m):

$$X_v = -b/2a + \sqrt{b^2 - 4ac}/2a$$

After substituting X_p from Eq. (25) into Eq. (28):

$$X_v = -b \bigg/ 2a + \sqrt{b^2 - 4a\left[X_m^2\bigg/(\cos\beta)^2 - \left(-D_c\bigg/2 + \sqrt{D_c^2 + 4A/\pi}/2\right)^2\right]}\bigg/2a \tag{29}$$

The nozzle geometry and dimensions displayed in Figure 5 can be used to obtain the geometrical relationship in terms of measurable dimensions as,

$$H_o = H_t - t - (X_v - X_m)\tan\beta \tag{30}$$

In Case II, H_o should confirm the condition; $Y_{max} \leq H_o \leq H_{max} + t$.

Table 2. Predicted DR, X_p and A_{min} at air cap settings P1 to Pmax for Schlick 970 Form 4.

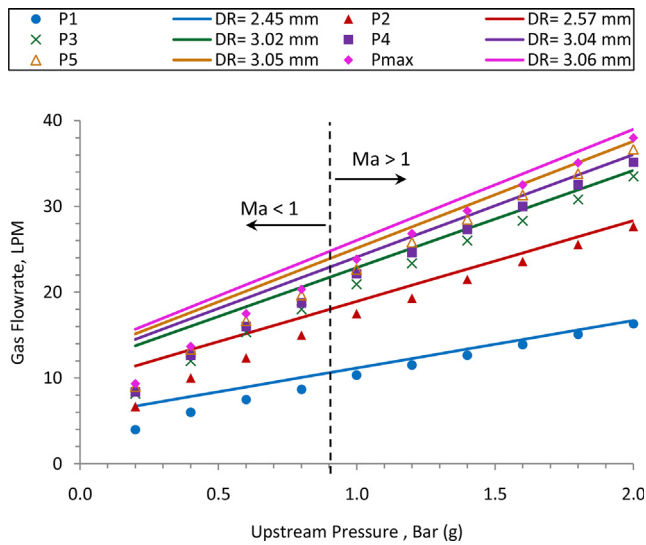| Air cap Position	Distance Ring Height DR, mm	Throat Gap Size Xp, mm	Amin, mm^2
P1	2.45	0.08	0.47
P2	2.57	0.14	0.80
P3	3.02	0.18	0.97
P4	3.04	0.19	1.02
P5	3.05	0.20	1.06
Pmax	3.06	0.21	1.10

Figure 8. Comparison of the predicted gas flow rates (Lines) with the nozzle supplier data [15] at P1 to Pmax (symbols) as a function of applied dispersion gas pressures up to 2 bars

After substituting X_v in Eq. (30) and replacing A with A_{min},

$$H_o = H_t - t -$$

$$\left[-b \Big/ 2a + \sqrt{ b^2 - 4a \left[X_m{}^2 \Big/ (\cos\beta)^2 - \left(-D_c \Big/ 2 + \sqrt{D_c{}^2 + 4A_{min}/\pi/2} \right)^2 \right] } \right]$$

$$\Big/ 2a - X_m \Big] \tan\beta \tag{31}$$

Finally, Eq. (22) or (31) and the relationship between H_o and A_{min} can be used to adjust the nozzle throat gap X, and maintain the flow at the nozzle throat away from the choking conditions for a specified pressure drop. The distance ring height (DR) for the new condition can be calculated by using a reference distance ring as:

$$DR_{new} = DR_r + (H_{or} - H_{onew}) \tag{32}$$

where,

DR_{new}: new distance ring height needed for a new gas flow-rate at a specific pressure drop

DR_r: height of a reference distance ring

H_{or}: H_o for the nozzle with a reference distance ring DR_r

H_{onew}: calculated H_o using Eq. (22) or (31)

A validation study by using the data in Figure 2 was conducted to check the accuracy of the predicted distance ring height (DR). In order to validate Eq. (32), the first step is to find the minimum nozzle cross section area A_{min} by using the gas flow rate, versus the applied upstream pressure shown in the Figure 2. If our approach in section 2 is correct, the distance ring height that is calculated by using Eq. (32) should yield the same dimension with the standard distance ring that the nozzle comes with. Step by step details of this calculation and the other results given in this section can be found in the supplementary excel file.

3. Results and discussion

Our calculations showed that the distance ring height DR for position 4 is 3.04 mm, a close match with the 3.01 mm height of the standard distance ring height that came with the nozzle. After this verification, we calculated the cross section areas, throat sizes and distance ring heights for other positions (P1-Pmax), and results are presented in Table 2.

The next step is to calculate the gas flow rates by using the predicted DR heights, and comparing the results with the data given in Figure 2. An objective function E was defined as the difference between the calculated distance ring height at each step, and the heights as listed in Table 2 for positions P1 to Pmax. A Generalized Reduced Gradient (GRG) nonlinear algorithm was used in excel program to minimize the objective function, while the gas flow rate was set as the variable. Gas flow rate that would yield an E = 0 was then calculated by the solver, and the results are presented in Figure 7.

The difference between the predicted flow rates and the nozzle supplier data is small above 2 bar pressures. Pressures above 10 bars were not considered due to the deviation from the perfect gas assumption. However, a 10 bar pressure drop is more than enough for FSP operations. Figure 8 focuses at a low pressure range, and it is clearly seen that the deviation in flow rate below 1 bar pressure drop is above 70 %, as shown in Table 3. Large error at low pressures, especially at upstream pressures less than 2 bars is no surprise. According to Eq. (7),

Table 3. Percent error between the predicted gas flow rates and flow rates read from the nozzle supplier chart [15] as a function of the upstream pressure (P_u) at air cap settings P1 to Pmax.

P_u	% deviation in predicted flow rate					
Bar (gage)	P1	P2	P3	P4	P5	Pmax
0.2	68.1	71.1	68.6	72.5	68.2	68.1
0.4	30.6	32.9	33.7	33.5	32.3	33.8
0.6	19.2	23.0	19.4	20.6	20.8	19.2
0.8	16.0	13.7	14.3	15.7	15.0	15.3
1	8.0	8.2	9.2	8.7	10.3	9.3
1.2	6.7	7.9	7.6	7.6	6.9	6.7
1.4	5.6	5.5	5.3	5.6	5.7	5.8
1.6	4.3	4.2	4.6	4.2	4.1	4.0
1.8	3.4	3.5	3.5	3.6	3.8	3.7
2	2.3	2.4	2.1	2.5	2.5	2.6
3	0.4	0.5	0.5	0.3	0.5	0.5
4	0.5	0.5	0.3	0.3	0.4	0.5
5	0.5	0.5	0.3	0.3	0.6	0.5
6	0.4	0.4	0.3	0.3	0.5	0.5
7	0.4	0.3	0.3	0.3	0.7	0.5
8	0.4	0.3	0.3	0.3	0.4	0.5
9	0.3	0.3	0.3	0.3	0.5	0.5
10	0.5	0.3	0.3	0.3	0.4	0.3

Table 4. Predicted distance ring heights by Eq. (32) and error in pressure drop.

O$_2$ gas flow rate, LPM	Required Pg, Bar	Predicted DR, mm	Experimental Pg, Bar	% Error in Pg, Bar
5	1.0	2.37	0.92	8.7
5	1.5	2.35	1.43	4.9
10	1.0	2.44	0.92	8.7
10	1.5	2.41	1.43	4.9

to maintain the nozzle throat at sonic conditions, the upstream pressure P_u must be above the critical pressure $P_c = P_d/0.5283$, where P_d is the downstream pressure (1 bar) [16]. Therefore, at upstream pressures less than 1.89 bars (absolute), Ma < 1, the gas velocity is below sonic speed, and supersonic above 2 bars. The assumption in the derivation of our equation is not valid below 2 bars, and isentropic flow approximation does not hold. The error is in between 8 to 10% above 2 bars, and becomes much smaller after 3 bars.

Results show that, with the distance ring height calculation method suggested here, the nozzle can be operated under conditions that are not provided in the supplier charts, without the need for time consuming and costly experimental trial and error methods. Additionally, one can easily calculate the flow rate to achieve the same pressure drop with a much smaller amount of gas with the same spray properties, achieving a more economical production. For example, the minimum amount of gas needed would be 14 LPM for an applied pressure of 1.5 bars according to the lowest standard nozzle position P1. However, by the method presented here, one can easily calculate that, with a distance ring of 2.35 mm, the same pressure drop can be achieved with a 5 LPM gas flow. After validation of our approach, the required distance ring heights for 5 and 10 LPM oxygen flows at 1 and 1.5 bars to produce TiO$_2$ were calculated and given in Table 4. The pressure drop for the distance rings in Table 4 was also measured experimentally, and the error in prediction was found to be about 9 % at 1 bar and 5 % at 1.5 bars. Nano-TiO$_2$ productions with an average primary particle diameter of 20 nm were successfully done with the distance rings that were determined by the technique presented here.

4. Conclusions

A simple mathematical expression was developed using the external measurable dimensions of a two phase external mixing nozzle, in order to set the spray properties at a desired flow rate and pressure drop. The error in predictions was found to be higher at applied pressures less than 2 bars, due to the isentropic gas approximation failing at pressure drops less than 0.89 bar and Ma < 1. Nozzle gap size and cross sectional area were calculated for a commercial nozzle, and validated by using the supplier chart for the nozzle positions P1 to Pmax [15]. The results revealed that the equation predicts nozzle settings well within the range of $2 < P_u \leq 10$ bars, which is sufficiently high for pilot scale production rates such as the one studied by Torabmostaedi et al. [18]. By using the derived Eq. (32), the user can adjust the air cap setting close enough to the targeted applied pressure and flow rate required for their application, ultimately saving time in the number of trial and errors otherwise needed. The method discussed here also allows utilization of a commercial two phase external nozzle beyond the ranges presented in the standard supplier charts, as well as providing information on gap size, which is necessary information in geometry meshing in computational fluid dynamics studies of FSP.

Declarations

Author contribution statement

Mustafi. A. Alhaleeb: Conceived and designed the experiments; Performed the experiments; Analyzed and interpreted the data; Contributed reagents, materials, analysis tools or data.

Nesrin. E. Machin: Conceived and designed the experiments; Performed the experiments; Analyzed and interpreted the data; Contributed reagents, materials, analysis tools or data; Wrote the paper.

Competing interest statement

The authors declare no conflict of interest.

Additional information

Supplementary content related to this article has been published online at https://doi.org/10.1016/j.heliyon.2020.e04840.

References

[1] W.Y. Teoh, R. Amal, L. Madler, Flame spray pyrolysis: an enabling technology for nanoparticles design and fabrication, Nanoscale 2 (2010) 1324–1347.

[2] L. Madler, H.K. Kammler, R. Mueller, S.E. Pratsinis, Controlled synthesis of nanostructured particles by flame spray pyrolysis, J. Aerosol Sci. 33 (2002) 369–389.

[3] L. Madler, S.E. Pratsinis, Bismuth oxide nanoparticles by flame spray pyrolysis, J. Am. Ceram. Soc. 85 (7) (2002) 1713–1718.

[4] W.J. Stark, R. Strobel, D. Günther, S.E. Pratsinis, A. Baiker, Flame-made titania/silica doped with transition metals: structural properties and catalytic behavior in epoxidation, J. Mater. Chem. 12 (2002) 3620–3625.

[5] G.L. Chiarello, I. Rossetti, L. Forni, Flame-spray pyrolysis preparation of perovskites for methane catalytic combustion, J. Catal. 236 (2005) 251–261.

[6] R. Strobel, A. Baiker, S.E. Pratsinis, Aerosol flame synthesis of catalysts, Adv. Powder Technol. 17 (2006) 457–480.

[7] G.L. Chiarello, I. Rossetti, L. Forni, P. Lopinto, G. Migliavacca, Solvent nature effect in preparation of perovskites by flame pyrolysis 2. Alcohols and alcohols + propionic acid mixtures, Appl. Catal., B 72 (2007) 227–232.

[8] B. Schimmoeller, F. Hoxha, T. Mallat, F. Krumeich, S.E. Pratsinis, A. Baiker, Fine tuning the surface acid/base properties of single step flame-made Pt/alumina, Appl. Catal., A 374 (2010) 48–57.

[9] S.E. Pratsinis, Aerosol-based technologies in nano-scale manufacturing: from functional materials to devices through core chemical engineering, AIChE J. 56 (2010) 3028–3035.

[10] R. Koirala, S.E. Pratsinis, A. Baiker, Synthesis of catalytic materials in flames: opportunities and challenges, Chem. Soc. Rev. 45 (2016) 3053.

[11] G. Solero, Synthesis of nanoparticles through flame spray pyrolysis: experimental apparatus and preliminary results, Nanosci. Nanotechnol. 7 (1) (2017) 21–25.

[12] Schlick atomizing technologies, Internet site accessed on April 2, 2020, www.myschlick.com/fileadmin/user_upload/Downloads/Informationsmaterial/04_TwoSubstance_970.pdf.

[13] S. Sel, O. Duygulu, U. Kadiroglu, N.E. Machin, Synthesis and characterization of nano-V$_2$O$_5$ by flame spray pyrolysis, and its cathodic performance in Li-ion rechargeable batteries, Appl. Surf. Sci. 318 (2014) 150–156.

[14] S. Ataol, A. Tezcaner, O. Duygulu, D. Keskin, N.E. Machin, Synthesis and characterization of nano-sized calcium phosphates by flame spray pyrolysis, and their effect on osteogenic differentiation of stem cells, J. of. Nanoparticle Res. (2015).

[15] Schlick Atomizing Technologies 2018, Operating instructions for Schlick two-substance nozzle model 970 form 4 S32, Internet site accessed on April 1, 2020, https://www.yumpu.com/en/document/view/63245092/04-twosubstance-970-flow-diagram.

[16] F.M. White, Fluid Mechanics, E- McGraw-Hill, New York, 2011, pp. 618–625.

[17] H. Lefebvre, V.G. McDonell, Atomization and Sprays, E- Taylor & Francis Group, New York, 2017, pp. 133–177.

[18] H. Torabmostaedi, T. Zhang, Computational study of the effect of processing parameters on the formation and growth of ZrO$_2$ nanoparticles in FSP process, Chem. Eng. Process 78 (2014) 1–10.